Nano Convergence

FULL PAPER

Open Access

TEPA impregnation of electrospun carbon nanofibers for enhanced low-level CO_2 adsorption

Jie Wang[1], Adedeji Adebukola Adelodun[2], Jong Min Oh[1] and Young Min Jo[1*]

Abstract

The CO_2 adsorption selectivity of plain activated carbon nanofibers (ANF) is generally low. For enhancement, nitrogen functionalities favorable for CO_2 adsorption are usually tethered to the ANF. In the current study, we adopted chemical impregnation using 0.5 wt% tetraethylenepentamine (TEPA) solution as an impregnant. To enhance the impregnation of TEPA further, preliminary oxidation of the nanofibers with 70% HNO_3 was conducted. The effects of HNO_3 and TEPA treatments on the modified ANFs were investigated for physical (using N_2 monosorb, thermogravimetric analyzer, scanning electron microscopy) and chemical (X-ray photoelectron spectrometer) changes. From the results, we found that although TEPA impregnation reduced the specific surface area and pore volume of the ANFs (from 673.7 and 15.61 to 278.8 m^2/g and 0.284 cm^3/g, respectively), whereas the HNO_3 pre-oxidation increased the number of carboxylic groups on the ANF. Upon TEPA loading, pyridinic nitrogen was tethered and further enhanced by pre-oxidation. The surface treatment cumulatively increased the amine content from 5.81% to 13.31%. Consequently, the final adsorption capacity for low (0.3%) and pure CO_2 levels were enhanced from 0.20 and 1.89 to 0.33 and 2.96 mmol/g, respectively. Hence, the two-step pre-oxidation and TEPA treatments were efficient for improved CO_2 affinity.

Keywords: Low CO_2 capture, Physical activation, Tetraethylenepentamine (TEPA), HNO_3 oxidation, Surface chemistry

1 Introduction

Besides the highest contributor to anthropogenic global warming, CO_2 could also be harmful at relatively low concentrations, especially in confined indoor spaces, depending on whether they are, stationary (such as offices, homes, and subway stations) or mobile environments (such as cars, airplane, and submarines) [1, 2]. Therefore, the control of indoor CO_2 at 1,000 ppm or higher concentrations [the limit set by the Environmental Protection Agency (EPA)] require efficient technologies for safe indoor activities with a long duration [3].

In the last two decades, indoor air quality (IAQ) researchers have intensified efforts to improve the adsorption of elevated levels of indoor CO_2. The use of amine-based or amine-functionalized adsorbents is popular among such research approaches [4]. Usually, these adsorbents are fabricated using grafting or the impregnation method [5]. Some researchers have confirmed that both impregnation and grafting are effective for increasing the CO_2 adsorption capacity of carbon-based sorbents [6–8]. Furthermore, Na Rao et al. [9] compared the two methods and their results showed that impregnation is superior to grafting with respect to amine-loading efficiency and eventual CO_2 adsorption capacity. Impregnation of amines is usually a wet process during which amines are physically adhered onto a support via non-covalent attachment to improve the affinity of the support for a target adsorptive [10]. For example, the effects of three types of organic amines (i.e., diethylenetriamine, triethylenetetramine, and tetraethylenepentamine (TEPA)) on CO_2 adsorption capacity has been

*Correspondence: ymjo@khu.ac.kr
[1] Department of Applied Environmental Science, Kyung Hee University, 1732, Deogyeong-daero, Giheung-gu, Yogin-si, Gyeonggi-do 17103, Republic of Korea
Full list of author information is available at the end of the article

Springer Open

© The Author(s) 2020. This article is licensed under a Creative Commons Attribution 4.0 International License, which permits use, sharing, adaptation, distribution and reproduction in any medium or format, as long as you give appropriate credit to the original author(s) and the source, provide a link to the Creative Commons licence, and indicate if changes were made. The images or other third party material in this article are included in the article's Creative Commons licence, unless indicated otherwise in a credit line to the material. If material is not included in the article's Creative Commons licence and your intended use is not permitted by statutory regulation or exceeds the permitted use, you will need to obtain permission directly from the copyright holder. To view a copy of this licence, visit http://creativecommons.org/licenses/by/4.0/.

reported [11]. The results showed that if TEPA was used as a chemical impregnant for a solid support, it could improve CO_2 adsorption of the support.

TEPA is a linear molecule bearing five amine groups per molecule: two primary amines (RNH_2) and three secondary amine (R_2NH) groups. The mechanism by which primary amine and secondary amine react with CO_2 are expressed in Eqs. (1) and (2), respectively [5]:

$$CO_2 + 2RNH_2 \leftrightarrow RNH_3^+ + RNHCOO^- \quad (1)$$

$$CO_2 + 2R_2NH \leftrightarrow R_2NH_2^+ + R_2NCOO^- \quad (2)$$

However, to achieve optimum wet impregnation, adequate knowledge of certain properties of the support such as the specific surface area, pore size, pore structure, and surface pH is essential. In general, a porous support with a relatively high specific surface area and large pore volume has a good potential for organic amine immobilization [11].

In this study, various activated nanofibers (ANFs) were prepared by either physical or chemical activation. Further, all the ANFs were impregnated with TEPA solution. To improve the TEPA loading, some ANFs were pre-oxidized with nitric acid solution prior to impregnation.

2 Experimentals

2.1 Consumable materials

Polyacrylonitrile (PAN, M.W.=150,000 mol/g), 70% nitric acid, and tetraethylene pentamine (TEPA, Reagent grade) were purchased from SIGMA-ALDRICH, Co. in Korea. *N*,*N*-dimethylformamide (DMF), potassium hydroxide, and ethanol solution were procured from DAEJUNG CHEMICALS & METALS CO., Seoul, Korea. All of the reagents were used as-received.

2.2 Preparation of PAN-based carbon nanofibers

First, two types of PAN solutions were prepared in weight ratios: (i) PAN/DMF solution (PAN:DMF=1:9) for physical activation and (ii) KOH/PAN/DMF solution (PAN:DMF:KOH=1:9:0.01–0.05) for chemical activation. Each polymer solution was electrospun at an inject velocity of 1.5 mL/h under 18 kV. The electrospun nanofiber was stabilized in an oven at 200 °C for 4 h before cooling to room temperature. Then, cooling it to room temperature, it was transferred into a tubular quartz reactor and heated at a ramping rate of 5 °C/min to 800 °C under N_2 flow that was fed at 200 cm. Samples prepared with weight ratios (i) were activated for 15, 30, 60 and 90 min, and denoted as 15-ANF, 30-ANF, 60-ANF, and 90-ANF, respectively, whereas those prepared with weight ratios (ii) were activated for 15 min, and similarly denoted as 0.01-ANF, 0.03-ANF, and 0.05-ANF. Furthermore, 0.5 wt% TEPA solution in absolute ethanol was prepared as an impregnating solution. Then, 100 mg of each sample was added to the solution, and stirred for 6 h at room temperature. Afterwards, the samples were evaporated to dryness in an oven. However, some of the ANFs were pre-oxidized with 70% HNO_3 solution at 80 °C for 1 h before TEPA impregnation. The HNO_3 pretreatment was preferably carried out below 100 °C for no more than 2 h [12]. Aside from ensuring a complete surface treatment of the fibers, the depth of the ravines increased and the fiber matrix remained uncorroded under those conditions.

2.3 Characterization of nanofiber adsorbent

The specific surface area (S_{BET}) and porosity of all the ANFs were measured by N_2 adsorption at 77 K using a surface analyzer (Belsorp mini II, BEL, Tokyo, Japan) at relative pressures (p/p_0) of 0–1. To pre-clean the samples prior to measurement, outgassing under N_2 flow for 3 h at 100 °C was carried out. The equation based on BET theory (Brunauer–Emmett–Teller) was used to calculate the S_{BET}, whereas the mesopore volume (V_{meso}) and micropore volume (V_{micro}) were obtained using Barrett–Joyner–Halenda (BJH) and MP-plot [5]. The total pore volume (V_{total}) was analyzed at a relative pressure of 0.99.

The thermal stability of the adsorbents was investigated with the aid of a thermogravimetric analyzer (TGA N-1500, Scinco, USA). Each sample was heated from room temperature to 400 °C at 10 °C/min heating rate under N_2 atmosphere. The surface morphology and feature of the samples were observed by field emission scanning electron microscopy (FE-SEM, LEO SUPRA 55, Germany) with the magnification of 50,000×. It was coupled with an energy-dispersive X-ray spectroscopy (EDS) for simultaneous elemental distribution analysis. In details, the changes in the surface chemical speciation, especially of the nitrogen functional groups, were investigated using X-ray photoelectron spectroscopy (XPS, K-Alpha, Thermo Scientific, USA).

2.4 Measurement of CO_2 adsorption capacity

The adsorption capacity of the adsorbents for pure CO_2 was obtained using a monosorb instrument. The measurement was carried out under pressures ranging from vacuum to ambient (i.e., p/p_0=0–1) at 273 K. Furthermore, the selective adsorption capacity for 0.3% CO_2 (99.999%, in binary mixture with 99.99% N_2) was examined using a lab scale set-up as shown in Fig. 1. The 0.3% (3000 ppm) CO_2 represents the mean concentration of the gas commonly found in indoor spaces [13]. A CO_2 detector (SenseAir, Sweden), equipped with a non-dispersive infrared (NDIR) sensor was used to monitor the CO_2 concentration in the exiting gas stream. The same

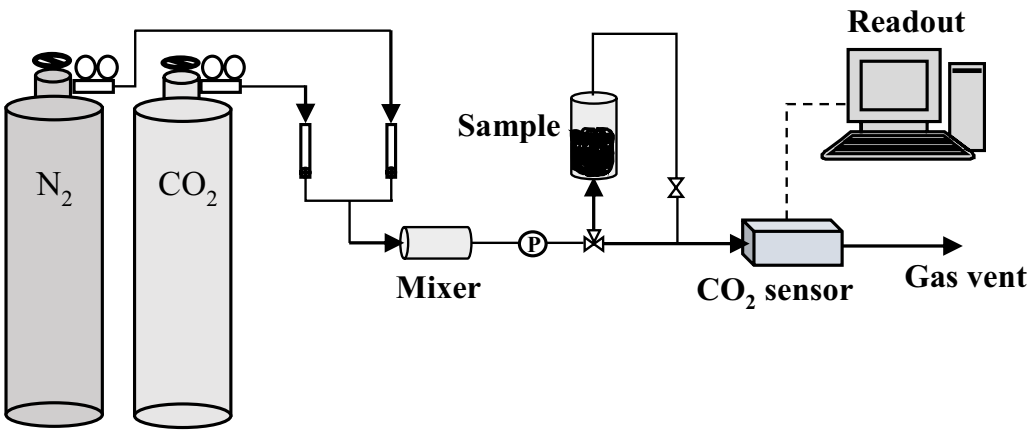

Fig. 1 A schematic diagram of the low-level CO_2 adsorption test set-up

set-up was used for adsorption regeneration exercise carried out at 100 °C.

3 Results and discussion

3.1 Physical properties of the ANFs

Table 1 shows the textural characteristics of all of the ANF samples. We observed that the S_{BET} and V_{total} of ANFs were enhanced by either activation time or the quantity of the activation reagent. However, after impregnation with TEPA, the S_{BET} and V_{total} were reduced proportionately, an observation that is consistent with those of other studies [11, 14]. In particular, micropores of the chemically activated ANFs undetectable because the percolation of the TEPA solution blocked the tiny pores. On the contrary, the microporosity of the ANFs derived by physical activation increased after impregnation, probably due to the thermal shrinking of boundary mesopores. Since the kinetic diameter of CO_2 is 0.33 nm, a factor that is significant to its physisorption, the proportion of microporosity is essential to the adsorption of the gas. Therefore, we inferred that ANFs prepared by physical activation are more suitable for surface modification by

Table 1 Surface textural and porous properties of all of the ANF samples

Sample	S_{BET} (m^2/g)	V_{total} (cm^3/g)	V_{meso} (cm^3/g)	V_{micro} (cm^3/g)	V_{micro}/V_{total} (%)
Physically activated ANF					
15-ANF	212.2	7.201	7.113	0.083	1.15
15-ANF-TEPA	60.98	0.490	0.487	0.010	2.04
30-ANF	308.4	7.882	7.802	0.137	1.74
30-ANF-TEPA	100.7	0.466	0.364	0.010	2.15
60-ANF	673.7	15.61	15.50	0.254	1.63
60-ANF-TEPA	249.2	0.207	0.190	0.047	22.5
60-ANF-HNO_3	583.7	0.463	0.295	0.229	49.4
60-ANF-HNO_3-TEPA	278.8	0.284	0.264	0.052	18.3
90-ANF	839.4	27.50	27.53	0.301	1.09
90-ANF-TEPA	113.0	0.246	0.170	0.015	6.01
Chemically activated ANF					
0.01-ANF	84.14	0.055	0.048	0.009	16.36
0.01-ANF-TEPA	26.64	0.040	0.046	ND	ND
0.03-ANF	184.3	0.112	0.108	0.025	22.51
0.03-ANF-TEPA	65.60	0.720	0.724	ND	ND
0.05-ANF	469.1	0.347	0.191	0.188	54.30
0.05-ANF-TEPA	50.17	1.445	1.393	ND	ND

ND not-detected

alkaline solution impregnation, which would improve the chemisorption of the CO_2 molecules.

The N_2 adsorption isotherms of a part of physically activated ANFs are compared in Fig. 2. All the isotherms followed a typical behaviour of Type I between 0 and 0.8 of the relative pressure, indicating single-layer reversible adsorption. Type I adsorption frequently occurs on microporous solids. The initial adsorption capacity is relatively large with the change of relative pressure, and then the adsorption capacity will not change greatly with the increase of relative pressure [15]. However, as P/Po approached 1, the adsorption capacity increased infinitely. This was caused by multiple molecular layers (physisorption) of the sorptive formed at various thicknesses on the solid surface, leading to the formation of Type II adsorption isotherm. Therefore, it can be seen that the ANFs prepared has both inner micropores and outer mesopores well developed.

To further enhance TEPA loading on the ANFs at the same impregnation concentration, the ANFs were oxidized with 70% HNO_3 solution for 1 h prior to TEPA impregnation. The HNO_3 oxidation formed crevasses and pits by eroding the graphene layer primarily from the basal planes of carbonaceous materials [16]. After HNO_3 oxidation, the surface became irregular and there were more oxygen-based active groups such as carboxyl, carbonyl and ether groups tethered onto the ANFs [17–19]. The presence of these active groups were advantageous for the attachment of TEPA onto the adsorbent surface via a displacement reaction [20, 21].

The optimization of HNO_3 pre-oxidation was conducted with 60-ANF because the textural quality (S_{BET} and V_{micro}/V_{total}) of the 60-ANF-TEPA sample was found best in the TEPA-impregnation step. After pre-oxidation, the V_{total} of 60-ANF decreased significantly from 15.61 to 0.463 cm^3/g. This was a result of mesopore shrinkage, resulting in a large increase in the proportion of micropore volume (V_{micro}/V_{total}) from 1.63 to 49.4%. The

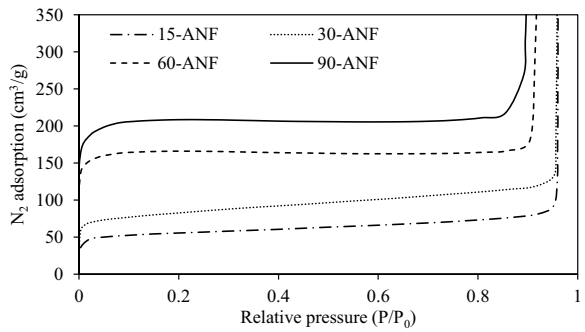

Fig. 2 N_2/77 K isotherm of physically activated ANFs

V_{micro}/V_{total} has been reported to be the driving force for selective adsorption of CO_2 [22]. Despite the significant improvement in this property, a slight decrease in the S_{BET} of the 60-ANF-HNO_3 sample was observed, which was attributed to the collapse of some mesopores. From the TEPA impregnation results of the adsorbent (before and after oxidation), the pre-treated 60-ANF-HNO_3-TEPA sample exhibited superior specific surface area and pore volume. However, the impregnation of TEPA depreciated the microporosity of the adsorbent (from 60-ANF-HNO_3 to 60-ANF-HNO_3-TEPA), i.e., a much superior microporosity was developed compared to that of 60-ANF. Finally, the pre-oxidized TEPA-doped ANFs showed more superior properties than those that were chemically activated.

The surface morphology of fibers is shown in the FE-SEM micrographs of ANFs (Fig. 3), produced at 50,000× magnification with 10 kV accelerating voltage. It can be seen that various surface modified ANFs exhibited uniform size distribution of fiber thickness. However, there were obvious etching on the surface of the TEPA-modified ANFs (Fig. 3b, d), while those of 60-ANF-TEPA sample (Fig. 3b) was deformed. Generally, the structural effects of HNO_3 pre-oxidation on the ANFs correspond with the differences in the S_{BET} and V_{total} of 60-ANF-HNO_3, which were higher than those of 60-ANF-TEPA and 60-ANF-HNO_3-TEPA (Table 1).

To understand the thermal stability of modified ANFs, we performed a thermogravimetric analysis on the samples. The thermograms obtained are shown in Fig. 4. All of the samples showed different rates of weight loss as the volatile organics and moisture content were eluted below 100 °C. TEPA-treated samples evinced a less steep slope than those that were untreated, indicating more refractiveness of the contents introduced by TEPA treatment. Between 100 and 400 °C, the 60-ANF sample showed the most impressive thermal stability, as a steady plateau was observed. Such steadiness could be attributed to the homogeneity of the fibers, devoid of foreign dopants in the matrix as can be seen in Fig. 3a. However, the thermogram of pre-oxidized fibers exhibited steeper depreciation because the oxidized fiber surfaces were more easily decomposed under an increasing temperature [20]. The strong acidic functionalities such as carboxylic, anhydrides and lactones tend to be decomposed at low temperatures, while the weak acidic functionalities such as carbonyl, phenol and quinone are dissipated at high temperature [23, 24]. The steady weight loss of TEPA impregnated samples (60-ANF-TEPA and 60-ANF-HNO_3-TEPA) began at about 180 °C. From the difference in their thermograms, we inferred that chemical modification was most pronounced on the surface of the pre-oxidized 60-ANF-HNO_3-TEPA sample.

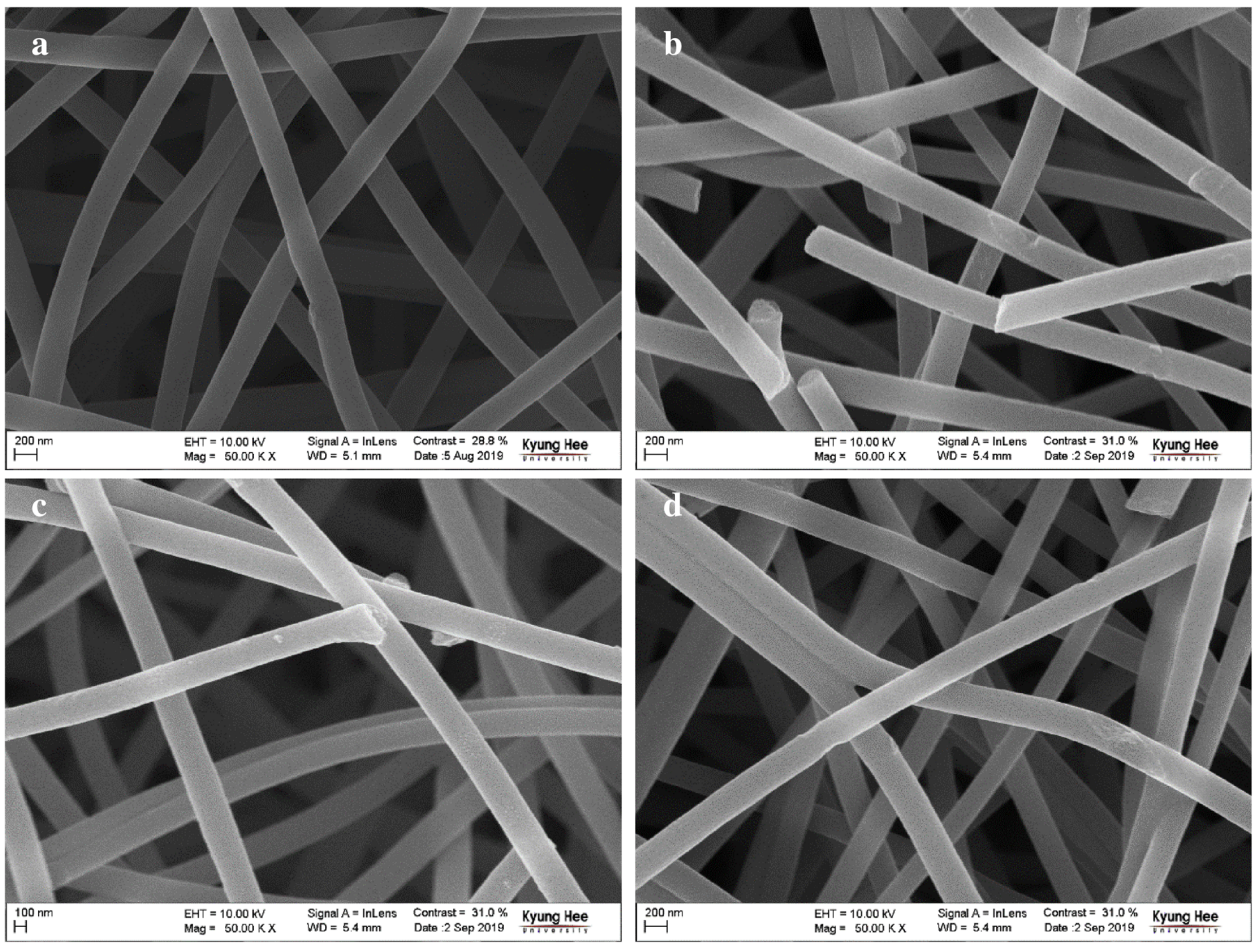

Fig. 3 FE-SEM images of **a** 60-ANF; **b** 60-ANF-TEPA; **c** 60-ANF-HNO_3; **d** 60-ANF-HNO_3-TEPA

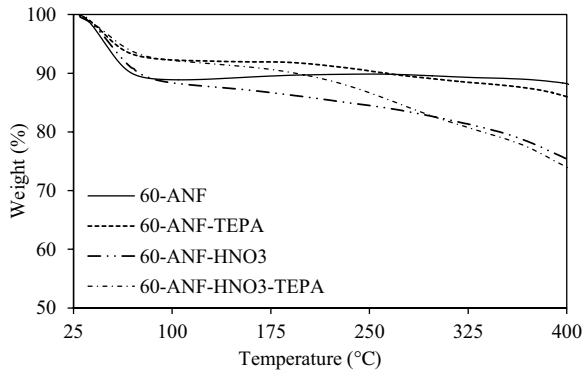

Fig. 4 Thermograms showing slopes that are indicative of the thermal stability of ANFs

3.2 Chemical properties of the ANFs

Through high resolution XPS analysis of the samples, the major peaks of the scan spectra determined to be due to the C_{1s}, O_{1s}, and N_{1s} photoelectrons. Table 2 lists the surface elemental compositions and atomic ratios of optimized 60-ANF samples. As expected, the HNO_3 treated sample (60-ANF-HNO_3) showed higher O_{1s}/C_{1s} ratios (14.75%) and N_{1s}/C_{1s} ratios (7.95%) than the unoxidized precursor (60-ANF). With HNO_3 treatment, the amount of O_{1s} and N_{1s} increased significantly, while

Table 2 The XPS-derived elemental compositions and atomic ratios of 60-ANF-based samples

Element (%)	Elementary composition (%)			Atomic ratio (%)	
	C_{1s}	O_{1s}	N_{1s}	O_{1s}/C_{1s}	N_{1s}/C_{1s}
60-ANF	89.02	5.16	5.82	5.80	6.54
60-ANF-TEPA	84.20	5.01	10.79	5.95	12.81
60-ANF-HNO_3	81.50	12.02	6.48	14.75	7.95
60-ANF-HNO_3-TEPA	77.41	9.28	13.31	11.99	17.19

the proportion of C_{1s} decreased due to surface eroding of the graphene layers, attributed to wet oxidation [25]. With the same impregnant concentration, the oxidized 60-ANF-HNO_3-TEPA sample showed a higher N_{1s}/C_{1s} ratios (17.19%) than that of the 60-ANF-TEPA (12.81%) sample, indicating that the HNO_3 oxidation treatment improved the loading of TEPA.

To better understand the chemical speciation of C and N on the selected samples, deconvolution of the XPS spectra was performed in the C_{1s} and N_{1s} regions. Figure 5 shows the best curve fit for the high resolution XPS C_{1s} spectra of all of the samples. Table 3 provides the percentage composition of the functional groups in the C_{1s} regime as (i.e. C in polyaromatic structures (C (sp^2), BE = 284.6 eV) or aliphatic structures (C (sp^3), BE = 285.4 eV): in phenolic, alcohol, ether or C=N groups (BE = 286.0 eV): in carbonyl or quinone groups (BE = 287.6 eV): and in carboxyl, lactone, or ester groups (BE = 288.8 eV) [26]. With either HNO_3 or TEPA treatment, the appearance of –OH and C=O groups on the fiber surface resulted in a decrease in the relative proportion of C (sp^2) and C (sp^3). Wet oxidation often incorporates high amount of oxygen, as carboxylic and phenolic functionalities on the carbon surface [20]. As expected, upon HNO_3 oxidation (60-ANF-HNO_3), the amount of –COOH groups increased significantly. However, the content of –COOH groups in the TEPA impregnated 60-ANF-TEPA and 60-ANF-HNO_3-TEPA samples decreased by 0.4% and 2.87% respectively, compared to that of 60-ANF and 60-ANF-HNO_3. Of the two possible types of acidic reactive groups present on the surface (phenolic –OH and carboxylic –COOH), only the carboxyl groups could undergo a reaction with TEPA because both phenolic and aliphatic hydroxyl groups are essentially inert toward primary and secondary amino groups [27]. This result indicated the successful substitution reaction of the acidic oxygen functionalities by the N-bearing groups from TEPA.

Table 3 Quantitative results of the fits of the XPS C_{1s} region, given in % of total intensity

Sample	286.4 C (sp^2)	285.4 C (sp^3)	286.0 –OH	287.6 C=O	288.8 –COOH
60-ANF	71.64	26.56	–	–	1.80
60-ANF-TEPA	58.31	24.03	10.37	5.89	1.40
60-ANF-HNO_3	59.74	13.52	13.54	7.90	5.30
60-ANF-HNO_3-TEPA	49.61	22.58	15.43	9.94	2.43

The nature and amount of the N species tethered by the amination were investigated. Figure 6 shows the best curve fit for the high resolution XPS N_{1s} spectra of all samples, while Table 4 lists the percentage of nitrogen-containing functional groups. The primary surface nitrogen groups found on the ANFs

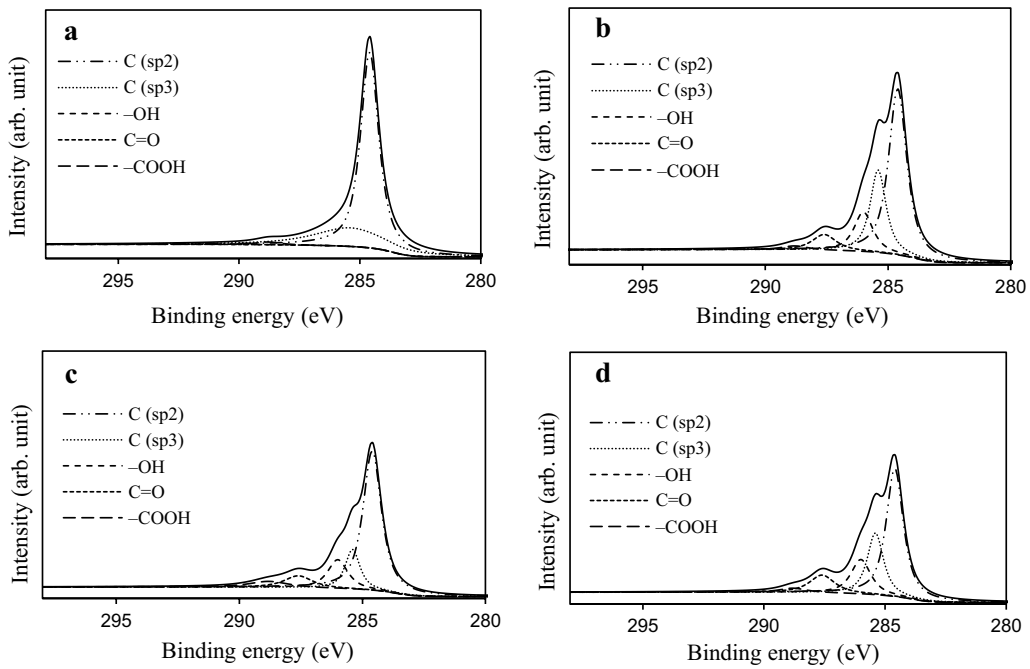

Fig. 5 The high resolution of the deconvoluted XPS C_{1s} spectra of the ANF samples: **a** 60-ANF; **b** 60-ANF-TEPA; **c** 60-ANF-HNO_3; and **d** 60-ANF-HNO_3-TEPA

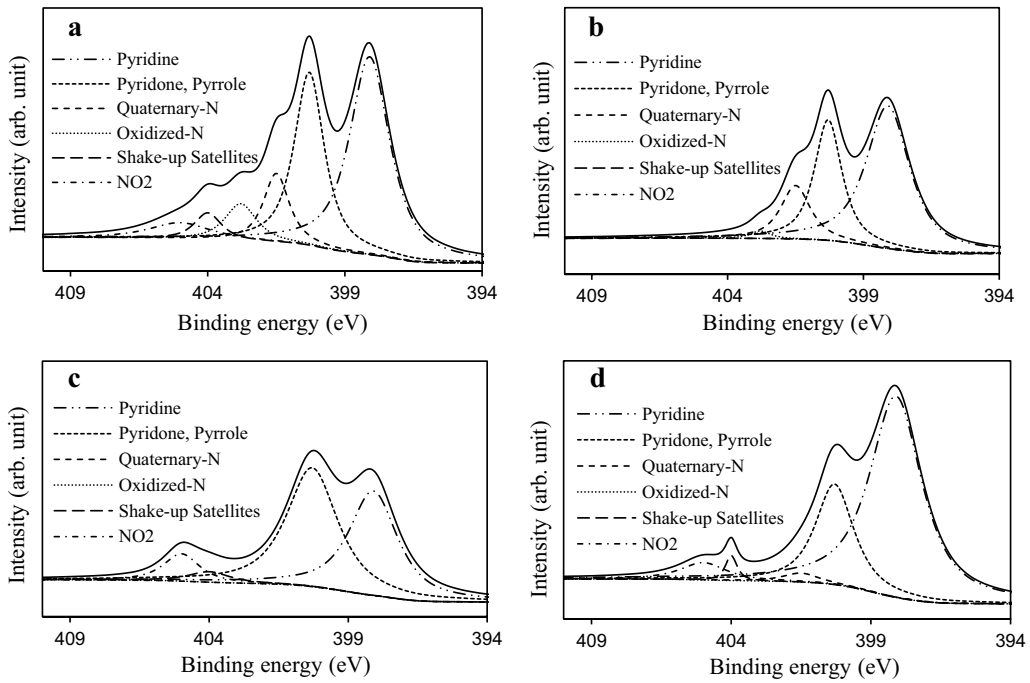

Fig. 6 The high resolution of deconvoluted XPS N_{1s} spectra of the ANF samples: **a** 60-ANF; **b** 60-ANF-TEPA; **c** 60-ANF-HNO_3; and **d** 60-ANF-HNO_3-TEPA

Table 4 Quantitative results of the deconvoluted XPS N_{1s} spectra values given in % of total intensity

Sample	398.1 eV Pyridine	400.3 eV Pyridone, Pyrrole	401.5 eV Quaternary-N	402.8 eV Oxidized-N	404 eV Shake-up satellites	405 eV NO_2
60-ANF	44.98	29.07	9.84	6.54	4.03	5.54
60-ANF-TEPA	55.48	29.30	13.92	1.30	–	–
60-ANF-HNO_3	40.38	48.34	-	–	3.46	7.82
60-ANF-HNO_3-TEPA	66.88	24.25	2.02	–	1.86	4.99

were pyridine-type (BE = 398.1 eV), pyridone and pyrrole (BE = 400.3 eV), quaternary-N (BE = 401.5 eV), oxidized-N (BE = 402.8 eV) [28], and chemisorption of NO_2 at 405 eV [14]. Pyridinic and pyridine/pyrrole N were the two dominant N-groups found on the 60-ANF. Both accounted for about 74% of the total N, while the other groups were present in minor to trace quantities. However, upon the impregnation of TEPA (60-ANF-TEPA), there was a significant increase in the pyridinic and quaternary N-groups, possibly derived from the total conversion of shake-up satellites and adsorbed NO_2. Such observation which implied that the linear TEPA resulted in the increase of pyridine-like structures or six-member or five-member rings [14]. As expected, HNO_3 oxidation evinced lowering of basic N-groups (pyridines), while the least basic groups (shake-up satellites and adsorbed NO_2) were re-introduced to the ANFs. Furthermore, final TEPA amination of the pre-oxidized samples (60-ANF-HNO_3-TEPA) ensured that the quantity of the desired pyridinic N was optimized, while the unwanted shake-up satellites and adsorbed NO_2 groups were significantly lowered. We concluded that although TEPA is a viable amination agent, it also incorporates refractory quaternary-N while expunging unwanted N groups. In addition, HNO_3 was confirmed as an excellent pre-oxidant for TEPA amination of ANFs, as it improved the tethering of preferred pyridine groups which are favorable for selective adsorption of CO_2 over N_2 [29].

To complement the elemental distribution analysis carried out with the XPS, an EDS analysis was performed on the optimized sample (60-ANF-HNO_3-TEPA). As shown in the Fig. 7, the EDS spectrum identified only a trace amount of N on the sample surface. Also, finite but

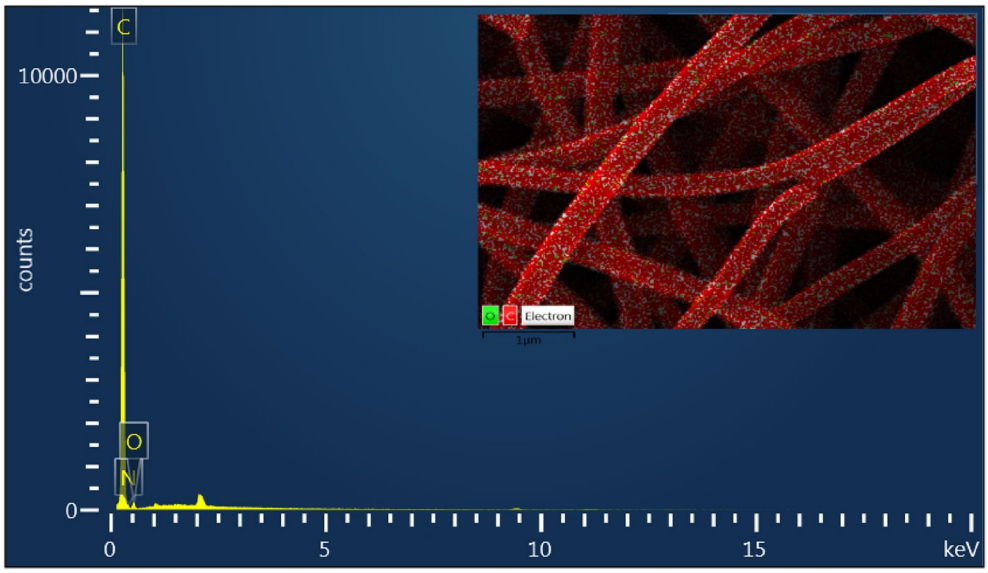

Fig. 7 The EDS spectrum of the sample 60-ANF-HNO3-TEPA (inset: EDS layered image)

uniform distribution of carbon and oxygen was observed. This was because XPS analysis is more sensitive than EDS, with a minimum detection concentration of 0.1%, although at the analysis depth of 10–20 nm only, while EDS analysis occurs bulk measurement that reaches micron level [30, 31]. Since the impregnated N-groups were populated on the surface of the adsorbent, the EDS analysis could only detect a lesser percentage compared to those of the XPS. Still, both measurements give comparatively similar results when compared in proportion.

4 Adsorption and regeneration of nanofiber adsorbents

4.1 CO_2 adsorption capacities of the ANFs

Table 5 shows the adsorption capacities for 0.3% and 100% CO_2 of all the test samples. We found that with either an increase in the activation time or the quantity of the activation reagent, the CO_2 adsorption capacity increased for both levels. This result is fundamentally true because gas adsorption is positively correlated with both the specific surface area and microporosity [32]. Although the S_{BET} of chemically activated ANFs was smaller than that of physically activated ANFs, the adsorption capacities of the former for pure CO_2 were still significantly improved. In regards to the 0.3% CO_2 test feed (Table 5), physically activated ANFs exhibited significantly higher adsorption capacities than their counterparts. We ascribed this result to the larger specific surface area induced by physical activation, which, in turn, favored TEPA impregnation and eventually CO_2 capture. In addition, the pre-oxidized 60-ANF-HNO_3-TEPA sample had higher amino loading (Table 2 and Fig. 4), resulting in the adsorption of 0.3% CO_2, which was about quadruple that of not pre-oxidized 60-ANF-TEPA.

Table 5 CO_2 adsorption capacities (q) of all ANF samples prepared in this work

Sample	CO_2 adsorption (mmol/g)	
	0.3%	100%
Physically activated ANF		
15-ANF	0.107	1.89
15-ANF-TEPA	0.034	0.65
30-ANF	0.151	2.10
30-ANF-TEPA	0.119	0.97
60-ANF	0.203	2.84
60-ANF-TEPA	0.087	1.48
60-ANF-HNO_3	0.121	1.98
60-ANF-HNO_3-TEPA	0.334	2.96
90-ANF	0.238	2.80
90-ANF-TEPA	0.117	1.00
Chemically activated ANF		
0.01-ANF	0.021	1.96
0.01-ANF-TEPA	0.015	0.33
0.03-ANF	0.028	2.67
0.03-ANF-TEPA	0.013	0.64
0.05-ANF	0.096	2.68
0.05-ANF-TEPA	0.020	0.41

Table 6 shows a comparison list of the CO_2 adsorption capacities of various adsorbents from open literatures.

Table 6 Comparison of the CO_2 adsorption capacities (q) of the current work with those from literature

Support	Modification chemicals	S_{BET} (m^2/g)	V_{micro}/V_{total} (%)	CO_2 feed level	CO_2 adsorption (mmol/g)	References
ANF	–	300	48	100%	2.74	[33]
	Urea 1:4	542	92	100%	2.98	[34]
Commercial ACF	10 wt% TEPA	1051	73	15%	0.50	[14]
CNTs	APTS	15.87	53	15%	0.98	[35]
ACF	HN_3 gas	1293	85	0.3%	0.40	[36]
AC	HN_3 gas	1251	–	10%	0.63	[37]
				0.3%	0.15	
ANF	0.5 wt% TEPA	278.8	18.3	0.3%	0.33	This work
				100%	2.96	

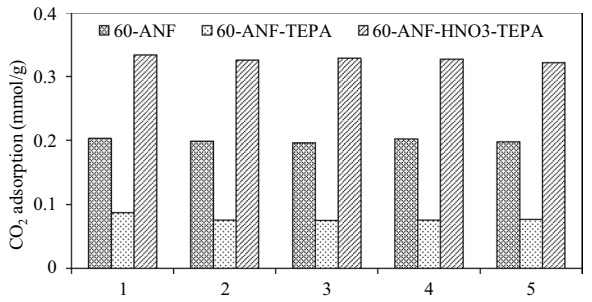

Fig. 8 Adsorption capacity of carbon dioxide in five cycles

For all the sorbents, the higher S_{BET} and V_{micro}/V_{total} were, the higher the adsorption capacity of pure CO_2 was. In our study, an increase in amino group content on the surface of the modified samples also led to a relatively high CO_2 adsorption capacity. However, as most published works have focused on pure and flue gas CO_2 levels, our work is unique in that we attempted to improve the CO_2 adsorption selectivity from indoor low levels.

4.2 Regeneration capacity of the ANFs

The regeneration of our representative samples for each treatment were examined by a simple temperature programmed desorption (TPD) using the TGA. The desorption temperature was set at 100 °C under N_2 atmosphere. It has been confirmed that the desorption of CO_2 form CO_2–TEPA interaction is likely occurred in two stages: (i) slow transport via the decomposition of primary ammonium–carbamate species, followed by (ii) rapid desorption of primary and secondary ammonium–carbamate species at 100 °C. At 100 °C, the ammonium–carbamate species was eliminated, which liberated most of the adsorbed CO_2 [38]. Figure 8 shows the 5-cycle regeneration adsorptions of CO_2 (3000 ppm). Quantitatively, the adsorption capacity of sample 60-ANF, 60-ANF-TEPA and 60-ANF-HNO_3-TEPA decreased mildly by 2.62%, 11.49% and 3.58% respectively, after 5 cycles. The regeneration performance of the TEPA impregnated samples was relatively weak, which may be caused by the thermal-induced elution of some TEPA molecules from the surface.

5 Conclusions

Nanofibers were prepared by electrospinning before physical or chemical activation to obtain activated nanofibers (ANFs) with varying structural and chemical characteristics. All of the ANFs were impregnated with a TEPA solution of varying amounts. By examination, we found that the ANFs that were physically activated were more suitable for TEPA impregnation because of the enhanced specific surface area and porosity. After TEPA impregnation, the specific surface area and total pore volume of the adsorbents decreased significantly. After the HNO_3 pre-oxidation treatment, the amine loading improved the incorporation of useful, basic pyridinic nitrogen, whereas the least basic N functionalities were effectively removed or converted. Therefore, the adsorption capacity of the optimized 60-ANF-HNO_3-TEPA for 0.3% and 100% CO_2 increased from 0.12 and 1.89 mmol/g (by 60-ANF-TEPA) to 0.33 and 2.96 mmol/g, respectively. A 5-cycle regeneration test showed a relatively stable adsorption of thermally refreshed adsorbents for proficient reusability. Consequently, HNO_3 pre-oxidation of TEPA-doped ANF is efficient for enhancing low-level CO_2 adsorption from indoor spaces.

Abbreviations

ANF: activated carbon nanofiber; TEPA: tetraethylenepentamine; EPA: Environmental Protection Agency; IAQ: indoor air quality; PAN: polyacrylonitrile; DMF: *N*,*N*-dimethylformamide; FE-SEM: field emission scanning electron microscopy; XPS: X-ray photoelectron spectroscopy; EDS: energy-dispersive X-ray spectroscopy; NDIR: non-dispersive infrared; ND: not-detected; IUPAC: International Union of Pure and Applied Chemistry; BE: binding energy; APTS: 3-aminopropyl-triethoxysilane; TPD: simple temperature programmed desorption.

Acknowledgements
This work was supported by the National Research Foundation of Korea (NRF) grant funded by the Korea government (MSIT, MOE) and (No. 2019M3E7A1113077).

Authors' contributions
JW completed the literature review, main experimental works and wrote the manuscript. AAA and JMO reviewed and edited the article, and YMJ designed the entire study including funding. All authors read and approved the final manuscript.

Funding
This work was supported by the Basic Science Research Program through the National Research Foundation of Korea (NRF) funded by the Korea government (MSIT, MOE) and (No. 2019M3E7A1113077).

Availability of data and materials
Not applicable.

Competing interests
The authors declare that they have no competing interests.

Author details
[1] Department of Applied Environmental Science, Kyung Hee University, 1732, Deogyeong-daero, Giheung-gu, Yogin-si, Gyeonggi-do 17103, Republic of Korea. [2] Centre for Renewable Energy Technology (CRET), The Federal University of Technology, P.M.B. 704, Akure, Nigeria.

Received: 9 October 2019 Accepted: 6 January 2020
Published online: 17 February 2020

References

1. Airqualitynews, CO_2 affects human health at lower levels than previously thought (2019). https://airqualitynews.com/2019/07/10/co2-affects-human-health-at-lower-levels-than-previously-thought.
2. R. Serna-Guerrero, A. Sayari, Modeling adsorption of CO_2 on amine-functionalized mesoporous silica. 2: kinetics and breakthrough curves. Chem. Eng. J. **161**, 182–190 https://doi.org/10.1016/j.cej.2010.04.042.
3. S.M. Saad, A.Y.M. Shakaff, A.R.M. Saad, A.M. Yusof, A.M. Andrew, A .Zakaria, A.H. Adom, Development of indoor environmental index: air quality index and thermal comfort index. AIP Conf. Proc. **1808**, 020043 (2017). https://doi.org/10.1063/1.4975276
4. N.Diez, P.Alvarez, M.Granda, C.Blanco, R.Santamaria, R.Menendez, CO_2 adsorption capacity and kinetics in nitrogen-enriched activated carbon fibers prepared by different methods. Chem. Eng. J. **281**, 704–712 (2015). https://doi.org/10.1016/j.cej.2015.06.126
5. Q.Ye, J.Q.Jiang, C.X. Wang, Y.M. Liu, H.Pan, Y.Shi, Adsorption of low-concentration carbon dioxide on amine-modified carbon nanotubes at ambient temperature. Energy Fuels. **26**, 2497–2504 (2012). https://doi.org/10.1021/ef201699w
6. P.J.E. Harlick, A.Sayari, Applications of pore-expanded mesoporous silicas. 3: Triamine silane grafting for enhanced CO_2 adsorption. Ind. Eng. Chem. Res. **45**, 3248–3255 (2006). https://doi.org/10.1021/ie051286p
7. J.Fujiki, K.Yogo, Carbon dioxide adsorption onto polyethylenimine-functionalized porous chitosan beads. Energy Fuels **28**, 6467– 6474 (2014). https://doi.org/10.1021/ef500975g
8. N. Chouikhi, J.A. Cecilia, E. Vilarrasa-García, S. Besghaier, M. Chlendi, F.I.F. Duro, E.R. Castellon, M. Bagane, CO_2 adsorption of materials synthesized from clay minerals: a review. Minerals **9**, 514 (2019). https://doi.org/10.3390/min9090514
9. N. Rao, M. Wang, Z.M. Shang, Y.W. Hou, G.Z. Fan, J.F. Li, CO_2 adsorption by amine-functionalized MCM-41: a comparison between impregnation and grafting modification methods. Energy Fuels **32**, 670–677 (2018). https://doi.org/10.1021/acs.energyfuels.7b02906
10. M.G. Plaza, C. Pevida, A. Arenillas, F. Rubiera, J.J. Pis, CO_2 capture by adsorption with nitrogen enriched carbons. Fuel **86**, 2204–2212 (2007). https://doi.org/10.1016/j.fuel.2007.06.001
11. J. Jiao, J. Cao, Y. Xia, L.Z. Zhao, Improvement of adsorbent materials for CO_2 capture by amine functionalized mesoporous silica with worm-hole framework structure. Chem. Eng. J. **306**, 9–16 (2016). https://doi.org/10.1016/j.cej.2016.07.041
12. J. Yang, L.X. Zhang, L. Zhou, X.J. Gong, Surface treatment of carbon fiber with nitric acid. Contemp. Chem. Ind. **44**, 2289–2293 (2015). https://doi.org/10.3969/j.issn.1671-0460.2015.10.005
13. A.A. Adelodun, J.C. Ngila, D.G. Kim, Y.M. Jo, Isotherm, thermodynamic and kinetic studies of selective CO_2 adsorption on chemically modified carbon surfaces. Aerosol Air Qual. Res. **16**, 3312–3329 (2016). https://doi.org/10.4209/aaqr.2016.01.0014
14. Y.C. Chiang, Y.J. Chen, C.Y. Wu, Effect of relative humidity on adsorption breakthrough of CO_2 on activated carbon fibers. Materials **10**, 1296 (2017). https://doi.org/10.3390/ma10111296
15. A.R. Barron, Physical methods in chemistry and nano science (cnx. org, 2012), p. 189–190.
16. C.U. Pittman Jr., G.R. He, B. Wu, S.D. Gardner, Chemical modification of carbon fiber surfaces by nitric acid oxidation followed by reaction with tetraethylenepentamine. Carbon **35**, 317–331 (1997). https://doi.org/10.1016/S0008-6223(97)89608-X
17. Y. Han, R. Li, C. Brückner, T.M. Vadas, Controlling the surface oxygen groups of polyacrylonitrile-based carbon nanofiber membranes while limiting fiber degradation. C J. Carbon Res. **4**, 40 (2018). https://doi.org/10.3390/c4030040
18. S. Tiwari, J. Bijwe, S. Panier, Tribological studies on polyetherimide composites based on carbon fabric with optimized oxidation treatment. Wear **271**, 2252–2260 (2011). https://doi.org/10.1016/j.wear.2010.11.052
19. L. Mahardiani, S. Saputro, F. Baskoro, N.M. Zinki, M. Taufiq, Facile synthesis of carboxylated activated carbon using green approach for water treatment. Mater. Sci. Eng. **578**, 012003 (2019). https://doi.org/10.1088/1757-899X/578/1/012003
20. M.S. Shafeeyan, W.M.A. Wan Daud, A. Houshmand, A. Shamiri, A review on surface modification of activated carbon for carbon dioxide adsorption. J. Anal. Appl. Pyrolysis. **89**, 143–151 (2010). https://doi.org/10.1016/j.jaap.2010.07.006
21. A.A. Adelodun, Y.H. Lim, Y.M. Jo, Effect of UV-C on pre-oxidation prior amination for preparation of a selective CO_2 adsorbent. J Anal. Appl. Pyrolysis **105**, 191–198 (2014). https://doi.org/10.1016/j.jaap.2013.11.004
22. M.S. Shafeeyan, W.M.A. WanDaud, A. Houshmand, A. Arami-Niya, Ammonia modification of activated carbon to enhance carbon dioxide adsorption: effect of pre-oxidation. Appl. Surf. Sci. **257**, 3936–3942 (2010). 10.1016/j.apsusc.2010.11.127.
23. J.L. Figueiredo, M.F.R. Pereira, M.M.A. Freitas, J.J.M. Orfao, Modification of the surface chemistry of activated carbons. Carbon **37**, 1379–1389 (1999). https://doi.org/10.1016/S0008-6223(98)00333-9
24. J.L. Figueiredo, M.F.R. Pereira, M.M.A. Freitas, J.J.M. Órfão, Characterization of active sites on carbon catalysts. Ind. Eng. Chem. Res. **46**, 4110–4115 (2007). https://doi.org/10.1021/ie061071v
25. B. Huang, G.W. Liu, P.H. Wang, X. Zhao, H.X. Xu, Effect of nitric acid modification on characteristics and adsorption properties of lignite. Processes **7**, 167 (2019). https://doi.org/10.3390/pr7030167
26. Y.C. Chiang, W.H. Lin, Y.C. Chang, The influence of treatment duration on multi-walled carbon nanotubes functionalized by H_2SO_4/HNO_3 oxidation. Appl. Surf. Sci. **257**, 2401–2410 (2011). https://doi.org/10.1016/j.apsusc.2010.09.110
27. J. March, *Advanced Organic Chemistry: Reactions, Mechanisms and Structure,* 3rd edn. (Wiley, New York, 1985)
28. G. Lim, K.B. Lee, H.C. Ham, Effect of N-containing functional groups on CO_2 adsorption of carbonaceous materials: a density functional theory approach. J. Phys. Chem. C **120**, 8087–8095 (2016). https://doi.org/10.1021/acs.jpcc.5b12090
29. Y.H. Lim, A.A. Adelodun, D.W. Kim, Y.M. Jo, Surface impregnation of glycine to activated carbon adsorbents for dry capture of carbon dioxide. Asian J. Atmos. Environ. **10**, 99 113 (2016). https://doi.org/10.5572/ajae.2016.10.2.099
30. A.G. Shard, Detection limits in XPS for more than 6000 binary systems using Al and Mg Kα X-rays. Surf. Interface Anal. **46**, 175–185 (2014). https://doi.org/10.1002/sia.5406
31. Energy dispersive X-ray microanalysis (EDX/EDS). https://www.andersonmaterials.com/edx-eds.html. Accessed 14 Dec 2019.
32. S.Y. Lee, S.J. Park, Determination of the optimal pore size for improved CO_2 adsorption in activated carbon fibers. J. Colloid Interface Sci. **389**, 230–235 (2013). https://doi.org/10.1016/j.jcis.2012.09.018

33. D.W. Kim, D.W. Jung, Y.M. Jo, Preparation of activated carbon fiber adsorbent for low level CO_2. J. Korean Soc. Atmos. Environ. **33**, 1–10 (2017). https://doi.org/10.5572/KOSAE.2017.33.1.001
34. D.W. Kim, D.W. Jung, A.A. Adelodun, Y.M. Jo, Evaluation of CO_2 adsorption capacity of electrospun carbon fibers with thermal and chemical activation. J. Appl. Polym. Sci. **134**, 45534 (2017). https://doi.org/10.1002/app.45534
35. F.S. Su, C. Lu, W. Cnen, H. Bai, J.F. Hwang ,Capture of CO_2 from flue gas via multiwalled carbon nanotube. Sci. Total Environ. **407** 3017–3023 (2009). https://doi.org/10.1016/j.scitotenv.2009.01.007
36. S.H. Hwang, D.W. Kim, D.W. Jung, Y.M. Jo, Impregnation of nitrogen functionalities on activated carbon fiber adsorbents for low-level CO_2 capture. J. Korean Soc. Atmos. Environ. **32**, 176–183 (2016). https://doi.org/10.5572/KOSAE.2016.32.2.176
37. A.A. Adelodun, Y.H. Lim, Y.M. Jo, Surface oxidation of activated carbon pellets by hydrogen peroxide for preparation of CO_2 adsorbent. J. Ind. Eng. Chem. **20**, 2130–2137 (2014). https://doi.org/10.1016/j.jiec.2013.09.042
38. W.C. Wilfong, C.S. Srikanth, S.S.C. Chuang , In situ ATR and DRIFTS studies of the nature of adsorbed CO_2 on tetraethylenepentamine films. ACS Appl. Mater. Interfaces **6**, 13617–13626 (2014). https://doi.org/10.1021/am5031006

Publisher's Note

Springer Nature remains neutral with regard to jurisdictional claims in published maps and institutional affiliations.

Submit your manuscript to a SpringerOpen journal and benefit from:

- ► Convenient online submission
- ► Rigorous peer review
- ► Open access: articles freely available online
- ► High visibility within the field
- ► Retaining the copyright to your article

Submit your next manuscript at ► springeropen.com